

---

This is an electronic reprint of the original article.  
This reprint may differ from the original in pagination and typographic detail.

Weigt, Dale; Korpi-Lagg, Maarit; Lagg, Andreas

**A novel technique for magnetic flux emergence diagnostics on the Sun**

Published: 01/09/2024

*Document Version*

Publisher's PDF, also known as Version of record

*Please cite the original version:*

Weigt, D., Korpi-Lagg, M., & Lagg, A. (2024). *A novel technique for magnetic flux emergence diagnostics on the Sun*. Poster session presented at UK Space Weather and Space Environment Meeting, Exeter, United Kingdom.

---

This material is protected by copyright and other intellectual property rights, and duplication or sale of all or part of any of the repository collections is not permitted, except that material may be duplicated by you for your research use or educational purposes in electronic or print form. You must obtain permission for any other use. Electronic or print copies may not be offered, whether for sale or otherwise to anyone who is not an authorised user.

# A novel technique for magnetic flux emergence diagnostics on the Sun

D. M. Weigt<sup>1</sup>, A. Korpi-Lagg<sup>2,1</sup>, M. J. Korpi-Lagg<sup>1</sup>

<sup>1</sup>Aalto University, Department of Computer Science, Finland; <sup>2</sup>Max Planck Institute for Solar System Research, Göttingen, Germany



Funded by the European Union



European Research Council  
Established by the European Commission

# A?

Aalto-yliopisto  
Perustieteiden korkeakoulu

## 1. Introduction

- Helioseismology allows us to analyse solar surface via oscillations of surface gravity waves: fundamental mode (*f*-mode).
- ***f*-mode is diagnostic for plasma flows and turbulent magnetic field structures** generated from magnetic flux advected from solar interior.<sup>1,2</sup>
- Previous studies found potential ***f*-mode enhancements a few days prior to  $t_0$** , the time of flux emergence<sup>3,4</sup>
- At times  $t > t_0$ , ***f*-mode is quenched** (as previously theorised).
- However these methods suffer from selection biases and key dependencies in background and heliocentric angle which affect the *f*-mode signal.
- Here, we create a novel method that eliminates the background dependence and normalises observations of interest using a time-dependent flat-field (FF).

## 2. Flat-field (FF) algorithm

- Use data products generated from *mtrack*\* applied to full-disk line-of-sight maps from Heliospheric Magnetic Imager (HMI) dopplergrams, using cylindrical plate carrée projection<sup>5</sup>
- **Korpi-Lagg+ 2022 pipeline<sup>6</sup>**, for full *mtrack* computation, calculates *k-v* maps for each 4-hr observation with resolution 0.05°, with solar lon/lat range  $\lambda_{\odot}, \psi_{\odot} = \pm 82.5^{\circ}, \pm 75^{\circ}$  producing full-disk 21x19 grid with 15° patches.
- **Algorithm can be summarised as follows:**

### 1) Point selection and patch tracking:

- Use *k*-nearest neighbours (KNN) computation to find closest 4 *k-v* maps to any  $(\lambda_{\odot}, \psi_{\odot})$  point.
- Use  $\lambda_{\odot}$  and Snodgrass and Ulrich (1990) empirical model to calculate solar rotation per 4-hr (i.e., track point for each observation)

### 2) FF calculation:

- Average over all *k-v* maps at  $(\lambda_{\odot}, \psi_{\odot})$  which follow the quiet Sun criterion<sup>6</sup>  $B_{RMS} \leq 20$  G
- Quiet maps are also subjected to thresholding on average wave power criterion to account for instrumental background (see Figure 1).
- Split into 4-hr intervals to remove 24-hr periodicity.

### 3) Calculation of *f*-mode power:

- Use a patch to locate sensible *f*-mode region from dispersion relation (see Figure 2).
- Normalise each observation at time *t* with associated FF, FF(*t*).
- Average over patch to find normalised *f*-mode power, or  $\mathcal{F}_r$ .

\*<http://hmi.stanford.edu/teams/rings/modules/mtrack/v25.html>

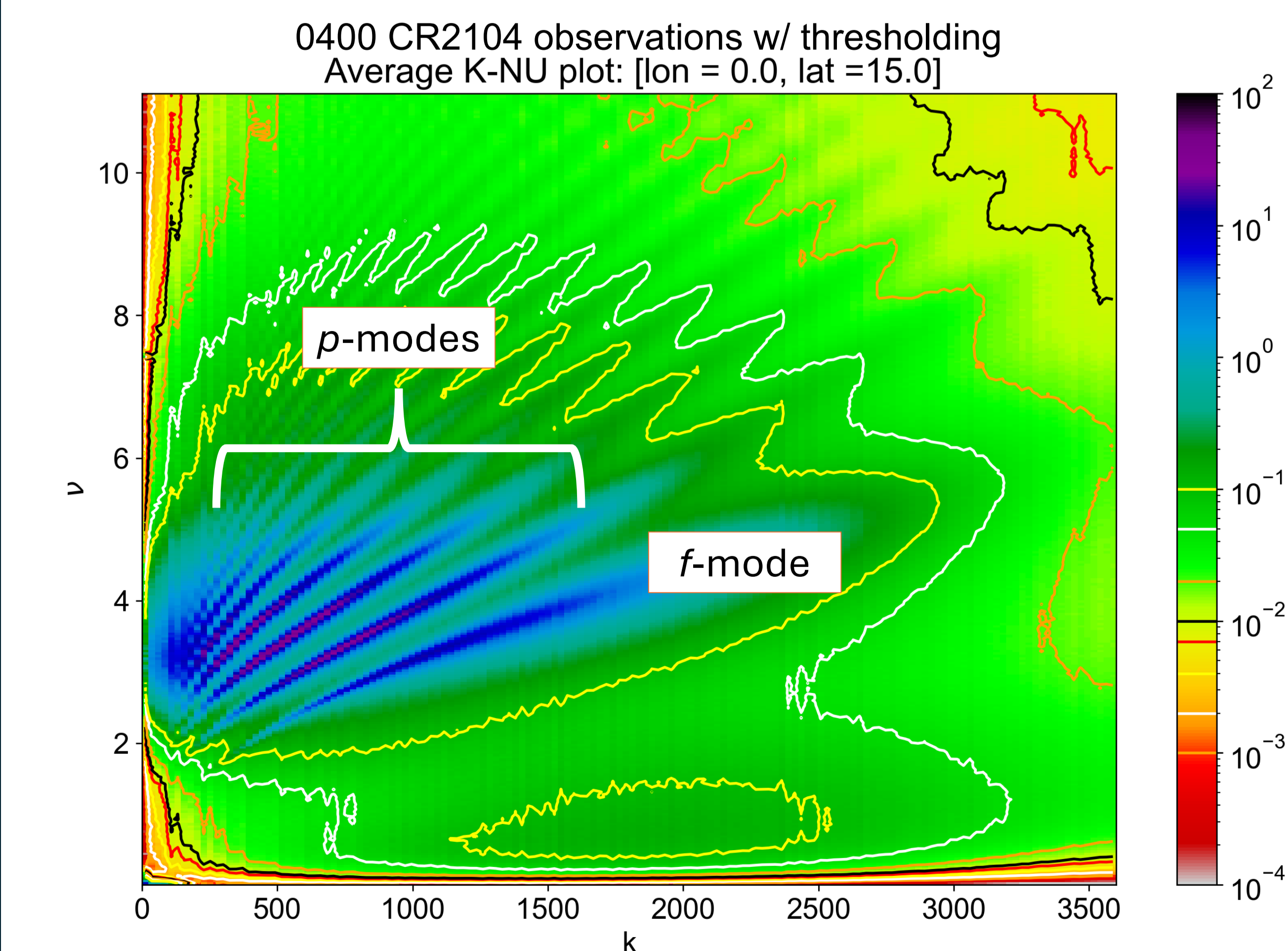


**Figure 1:** Labeled example of *k-v* FF map, using 0400 observations which follow threshold (over 28 day interval). Colour bar = power at each HMI pixel.

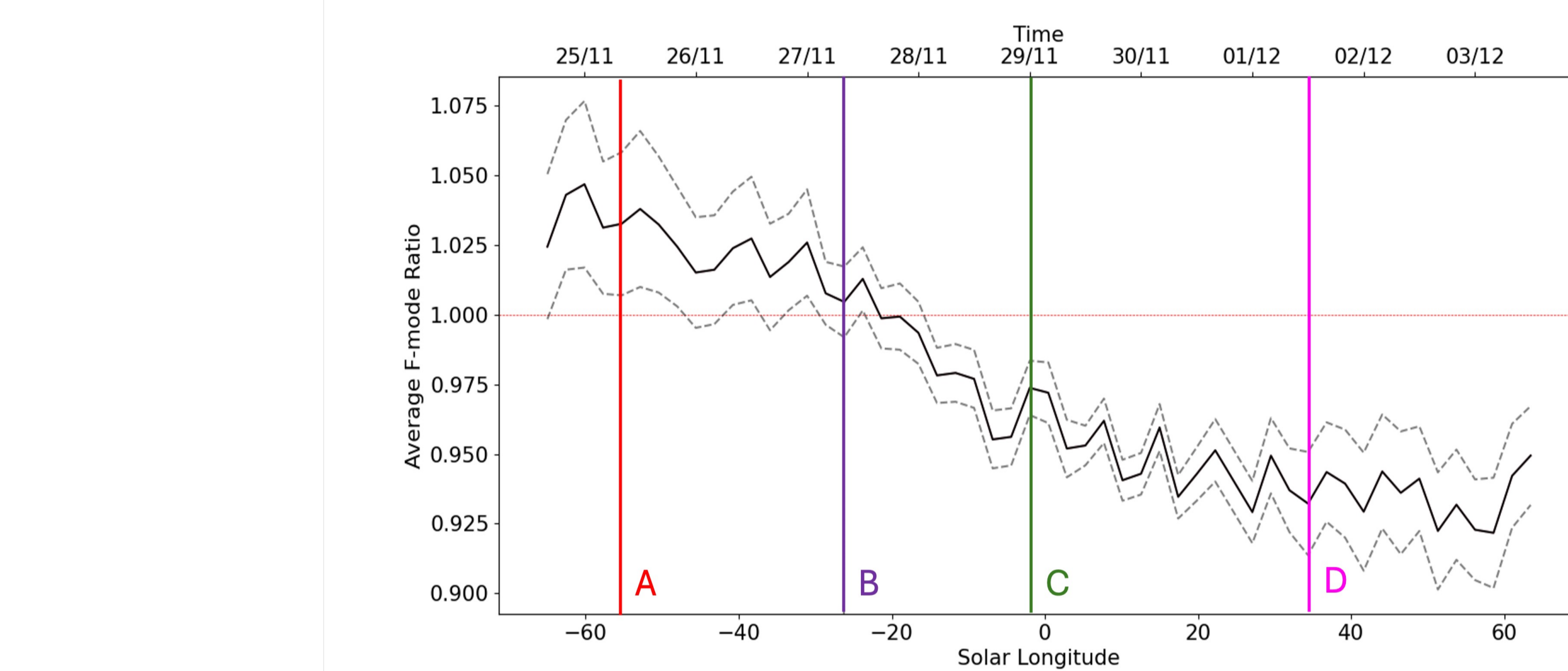
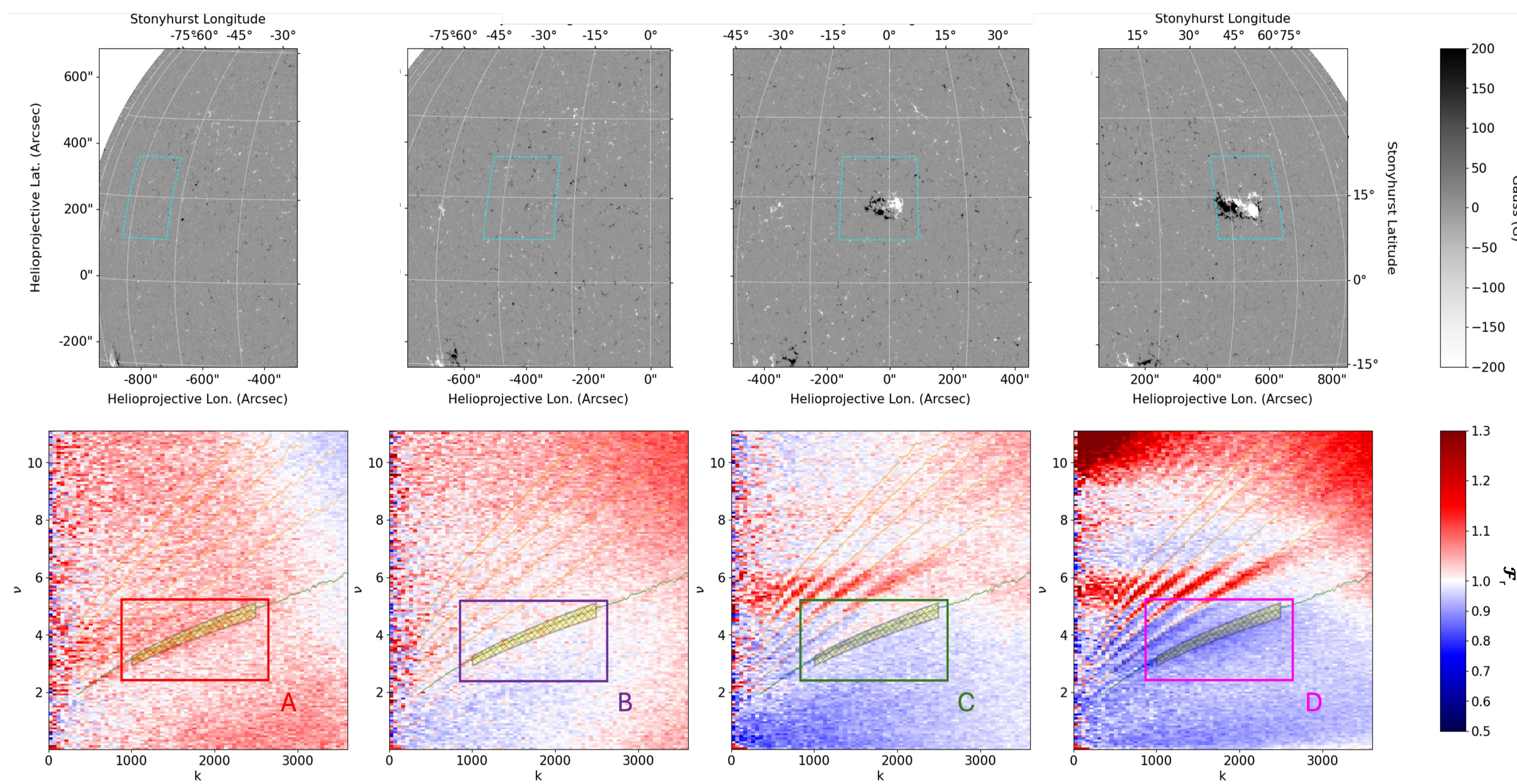


**Figure 2:** Plot showing four HMI images of the patch (cyan) tracking AR11130 across the disk. **A** = beginning,  $t < t_0$ ; **B** =  $t_0$  **this study**; **C** = National Oceanic and Atmospheric Administration (NOAA)  $t_0$  and **D** =  $t > t_0$  during observation interval with *k-v* diagram at each location using the FF method and the time evolution of  $\mathcal{F}_r$  (colour bar) with RMS error.

## 3. Interpretation of $\mathcal{F}_r$

- $\mathcal{F}_r > 1$ : enhancement of *f*-mode – caused by cavity size decreasing as flux approaches surface.
- $\mathcal{F}_r < 1$ : quenching of *f*-mode – caused by strong surface fields (large scale and turbulent) making region more rigid, inhibiting oscillations
- $\mathcal{F}_r \sim 1$ : unchanged behaviour from average, typical for undisturbed quiet Sun.

## 4. FF method key conclusions

- **FF method results compatible with theory<sup>1,2</sup>** (see Figure 2 example).
- **Choice of  $t_0$  critical for interpreting *f*-mode behaviour** – previous studies likely observed intervals of ‘higher quenching’ opposed to true enhancements.
- **Categorise behaviours using  $\mathcal{F}_r$**  (see Figure 3):

- (1) Quiet Sun (QS or  $\mathcal{F}_r \sim 1$ );
- (2) Populated region (PR; flux already emerged, or  $\mathcal{F}_r < 1$ );
- (3) Emerging active regions (QS/PR – behaviour shown in Figure 2);
- (4) Exceptional regions (ER; regions that exhibit behaviours outside these regimes, e.g., coronal holes: CHs)

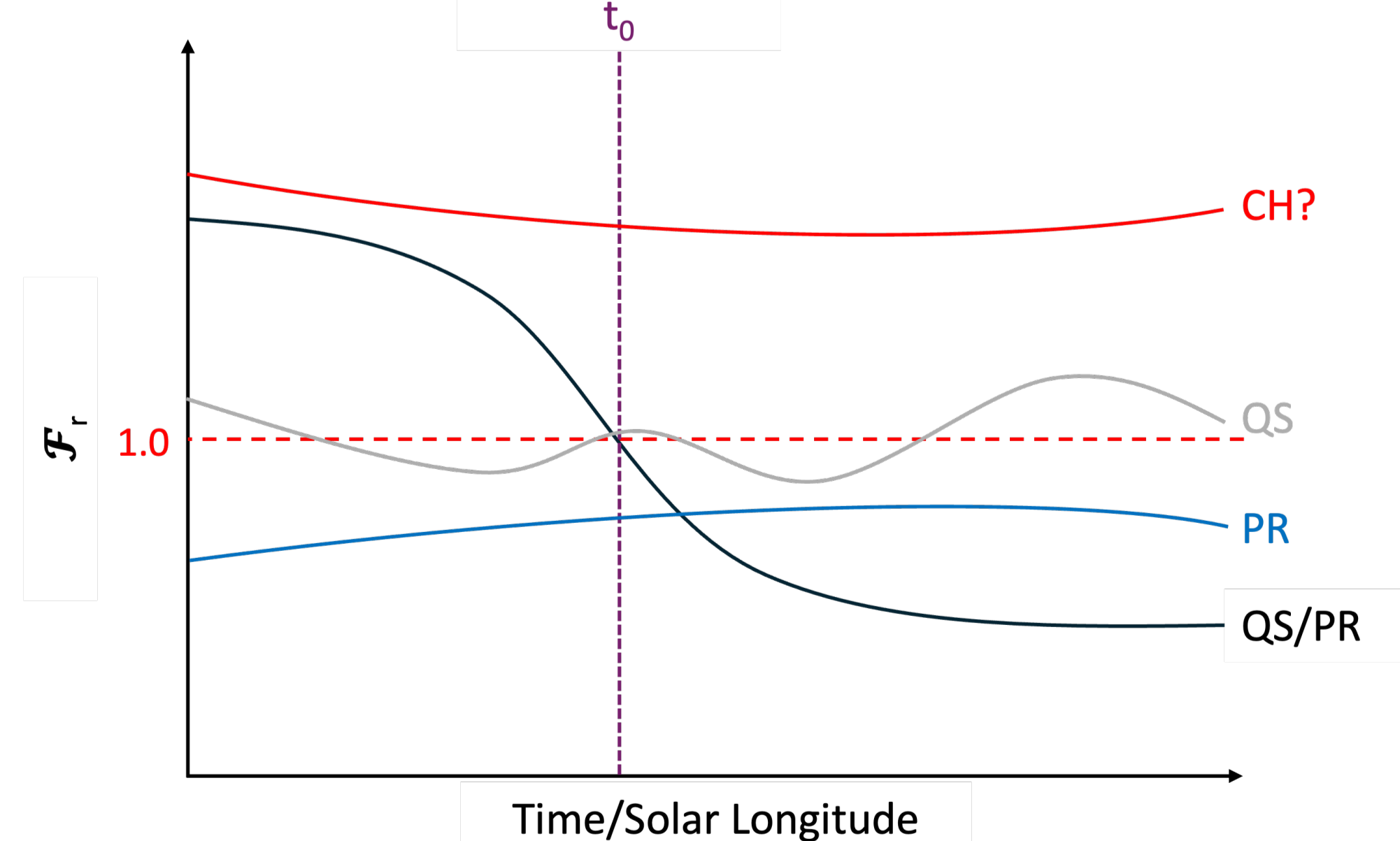


**Figure 3:** Schematic for general behaviours categorised by FF method. Labels can be utilised for machine learning/prediction purposes?

## 5. Next Steps

- Find a method and suitable parameter to utilise this for machine learning and prediction capabilities (Figure 3), and accurate diagnostics of time evolution.
- Compare with numerical modelling of magnetic flux advected to surface.
- **Paper in advanced preparation – publication soon!**

References:

<sup>1</sup>Duvall+ 1998, ApJ 505, L55, DOI: DOI 10.1086/311595; <sup>2</sup>Felipe+ 2012 ApJ 757 148 DOI: 10.1088/0004-637X/757/2/148; <sup>3</sup>Singh+ 2016 ApJ 832 120 DOI: 10.3847/0004-637X/832/2/120; <sup>4</sup>Waidele+ 2023 Sol. Phys. 298 30 DOI: 10.1007/s11207-023-02124-7; <sup>5</sup>Thompson 2006 A&A 449, 791-803 DOI: 10.1051/0004-6361:20054262; <sup>6</sup>Korpi-Lagg+ 2022 A&A 665, A141 DOI: 10.1051/0004-6361/202243979